AFRL-RX-WP-TR-2008-4228

TECHNICAL OPERATIONS SUPPORT (TOPS) II
Delivery Order 0007: Thermal Barrier Coatings

Universal Technology Corporation

FEBRUARY 2005
Final Report

AIR FORCE RESEARCH LABORATORY
MATERIALS AND MANUFACTURING DIRECTORATE
WRIGHT-PATTERSON AIR FORCE BASE, OH 45433-7750
AIR FORCE MATERIEL COMMAND
UNITED STATES AIR FORCE

NOTICE AND SIGNATURE PAGE

Using Government drawings, specifications, or other data included in this document for any purpose other than Government procurement does not in any way obligate the U.S. Government. The fact that the Government formulated or supplied the drawings, specifications, or other data does not license the holder or any other person or corporation; or convey any rights or permission to manufacture, use, or sell any patented invention that may relate to them.

This report was cleared for public release by the Air Force Research Laboratory Wright Site (AFRL/WS) Public Affairs Office (PAO) and is available to the general public, including foreign nationals. Copies may be obtained from the Defense Technical Information Center (DTIC) (http://www.dtic.mil).

AFRL-RX-WP-TR-2008-4228 HAS BEEN REVIEWED AND IS APPROVED FOR PUBLICATION IN ACCORDANCE WITH ASSIGNED DISTRIBUTION STATEMENT.

*//Signature//	//Signature//
MARK N. GROFF, Project Manager Thermal Sciences and Materials Branch Nonmetallic Materials Division	KENNETH A. FEESER Nonmetallic Materials Division Materials and Manufacturing Directorate

This report is published in the interest of scientific and technical information exchange and its publication does not constitute the Government's approval or disapproval of its ideas or findings.

*Disseminated copies will show "//Signature//" stamped or typed above the signature blocks.

REPORT DOCUMENTATION PAGE

Form Approved
OMB No. 0704-0188

1. REPORT DATE *(DD-MM-YY)*	2. REPORT TYPE	3. DATES COVERED *(From - To)*
February 2005	Final	15 May 2002 – 28 February 2005

4. TITLE AND SUBTITLE
TECHNICAL OPERATIONS SUPPORT (TOPS) II
Delivery Order 0007: Thermal Barrier Coatings

5a. CONTRACT NUMBER
F33615-01-D-5801-0007

5b. GRANT NUMBER

5c. PROGRAM ELEMENT NUMBER
62102F

6. AUTHOR(S)

5d. PROJECT NUMBER
4349

5e. TASK NUMBER
LO

5f. WORK UNIT NUMBER
4349L0T2

7. PERFORMING ORGANIZATION NAME(S) AND ADDRESS(ES)

Universal Technology Corporation
1270 N. Fairfield Road
Dayton, OH 45432

8. PERFORMING ORGANIZATION REPORT NUMBER

9. SPONSORING/MONITORING AGENCY NAME(S) AND ADDRESS(ES)
Air Force Research Laboratory
Materials and Manufacturing Directorate
Wright-Patterson Air Force Base, OH 45433-7750
Air Force Materiel Command
United States Air Force

10. SPONSORING/MONITORING AGENCY ACRONYM(S)
AFRL/RXOB

11. SPONSORING/MONITORING AGENCY REPORT NUMBER(S)
AFRL-RX-WP-TR-2008-4228

12. DISTRIBUTION/AVAILABILITY STATEMENT
Approved for public release; distribution unlimited.

13. SUPPLEMENTARY NOTES
PAO Case Number: AFRL/WS 05-1305, 01 Jun 2005. This report is the best quality available.

14. ABSTRACT
This work formed the second part of an investigation into the use of Gd203 as an alternative stabilizer for Zr02-based thermal barrier coating (TBC) materials. The current state-of-the-art TBC material, Y203-stablized Zr02 (3.5-4 mole percent y203), referred to as YSZ, suffers from limited durability at use temperature above 100-1200 °C. Our previous work investigated the influence of Gd203 concentration on the sintering and phase stability of conventional Zr02 powders. In this work, the effect of Gd203 concentration (420mol%) on the sintering and phase transformation of plasma-sprayed Zr02 powders was investigated and the data were compared with those for YSZ.

15. SUBJECT TERMS

16. SECURITY CLASSIFICATION OF:			17. LIMITATION OF ABSTRACT:	18. NUMBER OF PAGES	19a. NAME OF RESPONSIBLE PERSON (Monitor)
a. REPORT	b. ABSTRACT	c. THIS PAGE			Mark N. Groff
Unclassified	Unclassified	Unclassified	SAR	26	19b. TELEPHONE NUMBER *(Include Area Code)* N/A

Standard Form 298 (Rev. 8-98)
Prescribed by ANSI Std. Z39-18

TABLE OF CONTENTS

LIST OF TABLES

LIST OF FIGURES

LIST OF FIGURES (continued)

PREFACE

This technical report has been prepared as part of the requirements of the TOPS DO Contract Number 0007 with the Air Force Research Laboratory, Materials and Manufacturing Directorate, Wright-Patterson Air Force Base, Ohio. The report covers the work conducted during the period September 1, 2003 to February 28, 2005 and constitutes the final report under this contract.

ACKNOWLEDGEMENTS

The authors would like to thank the High Temperature Materials Laboratory (HTML), Oak Ridge National Laboratory (ORNL) for providing the facilities and equipment for thermal diffusivity measurements, and Dr. Hsin Wang for assistance with the measurements.

SUMMARY

This work formed the second part of an investigation into the use of Gd_2O_3 as an alternative stabilizer for ZrO_2-based thermal barrier coating (TBC) materials. The current state-of-the-art TBC material, Y_2O_3-stabilized ZrO_2 (3.5–4 mole percent Y_2O_3), referred to as YSZ, suffers from limited durability at use temperatures above 1000–1200 °C. Our previous work investigated the influence of Gd_2O_3 concentration on the sintering and phase stability of *conventional* ZrO_2 powders. In this work, the effect of Gd_2O_3 concentration (4–20 mol%) on the sintering and phase transformation of *plasma-sprayed* ZrO_2 powders was investigated and the data were compared with those for YSZ. Only the ZrO_2-4 mol% Gd_2O_3 and the YSZ compositions showed X-ray diffraction peaks characteristic of the metastable t′ phase. The ZrO_2-4 mol% Gd_2O_3 composition sintered more slowly and had a lower thermal conductivity than YSZ, but its resistance to destabilization of the t′ phase was lower than YSZ. Because of the reduced t′ phase stability, Gd_2O_3 by itself may not be an effective stabilizer for ZrO_2-based TBCs intended for high temperature use. Future work should investigate the sintering, phase stability, and thermal conductivity of co-doped ZrO_2 compositions simultaneously stabilized with Y_2O_3 and another rare-earth oxide such as Gd_2O_3.

1. INTRODUCTION

Thermal barrier coatings (TBCs) are used extensively to protect and insulate the metallic structure of jet aircraft engines and advanced gas turbine engines [1-8]. The current state-of-the-art TBC material, Y_2O_3-stabilized ZrO_2 (3.5–4 mol% Y_2O_3), referred to as YSZ, suffers from limited durability [6-8], particularly in applications that require prolonged exposure to high temperatures (above 1000–1200 °C). At these temperatures, YSZ undergoes sintering (or densification) [8-12], and transformation from the metastable tetragonal (*t′*) phase to the equilibrium tetragonal (*t*) phase, with the *t* phase undergoing a deleterious martensitic transformation to the monoclinic (*m*) phase [13-16]. Sintering and phase transformation provide additional failure mechanisms, and thereby contribute to reduced durability of the TBCs. Furthermore, sintering and phase stability issues will become of even greater significance in the design of future TBCs for use at higher temperatures. Therefore, an understanding of sintering and phase stability of ZrO_2-based TBCs will allow better utilization of these coatings and serve as a basis for the design of next-generation TBCs.

A previous report [17] provided the background and rationale for a compositional approach involving the use of alternative rare-earth oxide stabilizers for ZrO_2. Gadolinium oxide, Gd_2O_3, is one of the most effective stabilizers for reducing the thermal conductivity of ZrO_2 [18]. Since Gd^{3+} has a larger cation radius than Y^{3+} [19], the rate of diffusion-controlled processes such as sintering and *t′* phase transformation might be expected to be slower in Gd_2O_3-stabilized ZrO_2 than in YSZ. In previous work [17,20], which employed the use of *conventional* powders prepared by a co-precipitation route, the influence of Gd_2O_3 concentration on the sintering, grain growth, phase composition, and thermal conductivity of ZrO_2 was investigated. At an equivalent stabilizer concentration (4 mol%), Gd_2O_3 produced a lowering of the sintering, grain growth, and thermal diffusivity of ZrO_2 when compared to YSZ.

The objective of this work was to investigate the effect of Gd_2O_3 concentration (4–20 mol%) on the sintering, phase stability, and thermal conductivity of *plasma-sprayed* ZrO_2 and to com-

pare the data with those for plasma-sprayed YSZ. The majority of YSZ coatings prepared by the common TBC deposition processes (plasma spraying, PS, and electron beam physical vapor deposition, EB-PVD) have the metastable *t'* structure rather than the closely-related equilibrium *t* structure [13-16]. Therefore, studies on PS or EB-PVD material are warranted. The PS technique is used in this work because of the ready availability of equipment. The attainment and stability of the *t'* structure is of crucial importance for TBCs because the formation of the equilibrium *t* phase and its transformation to the *m* phase is accompanied by a volume change that leads to cracking and failure of the coating. In the experiments, coatings of Gd_2O_3-stabilized ZrO_2 and the baseline YSZ were deposited on high-purity graphite substrates. After removing the coatings from the substrate and grinding them to form a powder, the sintering and phase stability of the powders were studied. The thermal conductivity of dense discs prepared from the PS powders by hot pressing was also measured.

2. EXPERIMENTAL PROCEDURE

2.1 Preparation of Plasma Sprayed Powders

Plasma-sprayed (PS) powders of Gd_2O_3-stabilized ZrO_2 (4, 8, 12, and 20 mol% Gd_2O_3) and of the baseline YSZ (4 mol% Y_2O_3) were used in this work. Powders for the PS process were first synthesized by a conventional technique, described in detail elsewhere [17,20], and treated to provide the required range of particle (agglomerate) sizes for efficient flow through the PS gun. In this treatment, the conventionally-processed powder was calcined for 1 h at 1350 °C in a high purity Al_2O_3 crucible, ground with a diamonite mortar and pestle, and sieved through stainless steel sieves to produce dense agglomerates with particle sizes in the range of 53-75 μm. The powders were plasma-sprayed (Sulzer-Metco 9M; Winterthur, Switzerland), in a flame generated by an Ar/H_2 mixture, onto a high-purity graphite surface, to produce coatings with a thickness of ~0.5 mm. After removal from the graphite substrate by heating in air to 1000 °C and cooling, the free coating was ground to a powder using a hardened steel mortar and pestle, and passed through a 325-mesh sieve. The PS powder was washed twice with dilute HCl (1N) to remove metallic impurities, and twice with anhydrous ethanol, dried at 100 °C, lightly ground with a diamonite mortar and pestle, and passed through a 140-mesh nylon sieve. Samples of the powders were observed using scanning electron microscopy (SEM).

2.2 Sintering of Plasma-Sprayed Powders

Plasma-sprayed powders (Gd_2O_3-stabilized ZrO_2 and the baseline YSZ) were compacted in a 1/4-inch diameter steel die (applied pressure ≈ 250 MPa) to give pellets with a height of ~5 mm. The green density of the compacts, determined from the mass and dimensions, was 55–60% of the theoretical density. The compacts were sintered in air in a dilatometer (1600C; Theta Industries, Port Washington, NY), at a constant heating rate of 5 °C/min to 1400 °C. The tendency for sintering was determined from the axial shrinkage of the compact which was monitored continuously as a function of temperature. The fractured surfaces of compacts sintered for up to 40 h at 1400 °C were examined in the SEM in an effort to observe microstructural changes resulting from sintering.

2.3 Phase Composition and Phase Stability

The phases present in the as-prepared PS powders were studied using X-ray diffraction, XRD (Scintag; XDS 2000) with CuK_α radiation (λ = 1.5406 Å). After grinding in a diamonite mortar and pestle, and sieving through a 325-mesh stainless steel sieve, the powders were scanned stepwise in the range of 3–90° 2θ, at 0.03° per step, with a counting time of 0.5 second per step. The {111} and {400} peaks, in the range of 27-33° 2θ and 70-76° 2θ, were scanned more extensively, at 0.02° per step with a counting time of 15 seconds per step.

To investigate the stability of the phases, PS powders were heated in a high-purity Al_2O_3 crucible to 1400 °C, and held for 5, 10, 40, and 80 hours, after which they were cooled to room temperature (heating and cooling rate = 10 °C/min). A different powder sample was used for each run. The powders were analyzed by XRD using the same method described above for the as-prepared plasma-sprayed powders.

Quantitative XRD was performed to determine the concentration of phases present in the as-prepared and in the annealed PS powders. The integrated peak intensities of the XRD patterns were determined using software (RIQAS; Materials Data Inc., Livermore, CA). The mole fractions, *M*, of the *m*, *c*, and *t'* phases were determined from the calculated peak intensities, *I*, and using the most common equations, given by Miller *et al.* [13]:

$$\frac{M_m}{M_{c,t'}} = 0.82\frac{I_m(11\bar{1}) + I_m(111)}{I_{c,t'}(111)} \qquad \frac{M_c}{M_{t'}} = 0.88\frac{I_c(400)}{I_{t'}(400) + I_{t'}(004)} \tag{1}$$

2.4 Thermal Conductivity of Hot Pressed Discs

The thermal conductivity K′ was determined from separate measurements of the thermal diffusivity D and the specific heat capacity C_p, and using the equation:

$$K' = \rho D C_p \tag{2}$$

where ρ is the measured density of the sample. Because the samples were not fully dense, the thermal conductivity data were corrected for the residual porosity Φ of the samples, using the equation $K'/K = 1 - 4\Phi/3$, where K is the corrected thermal conductivity for the fully dense material [21].

Thermal diffusivity was measured using the laser flash technique [22,23]. Disc-shaped samples (15 mm in diameter × 1 mm) were machined from solid discs fabricated by hot pressing PS powders for 15 min at 1350 °C and 25 MPa pressure (heating and cooling rate = 10 °C/min). Prior to the measurement, the surfaces of the discs were coated with a thin layer of Ta, followed by a thin layer of C. Thermal diffusivity measurements were made at the High Temperature Materials Laboratory, Oak Ridge National Laboratory, at 100 °C intervals between 100 and 1000 °C (Anter Flashline 5000). For each sample, three measurements were taken at each temperature and the data was calculated using software (Anter FL5000). The heat capacity was measured

using differential scanning calorimetry, DSC (Netzsch) between 100 and 600 °C, in a nitrogen atmosphere, with Al as a standard. The sample consisted of a powder (<325 mesh), formed by grinding the hot pressed material.

3. RESULTS AND DISCUSSION

3.1 Sintering Kinetics of Plasma-Sprayed Powders

Figure 1 shows the linear shrinkage versus temperature for the sintering of plasma-sprayed (PS) powders of ZrO_2-4 mol% Gd_2O_3 and YSZ (ZrO_2-4 mol% Y_2O_3). For each composition, the data are the average for 2 runs under the same conditions. At any temperature, the shrinkage was reproducible to within 0.2%. The shrinkage is small, less than 5% for both samples, which may be explained in terms of the large particle size of the powders (< 45 μm). However, the data show that the Gd_2O_3-stabilized ZrO_2 composition sintered more slowly than YSZ. A similar trend was observed in previous work utilizing conventionally-processed powders [17,20]. The reduced sintering for the Gd_2O_3-stabilized ZrO_2 may be attributed to the slower diffusion of the larger Gd^{3+} ion (ionic radius = 0.105 nm), compared to Y^{3+} (ionic radius = 0.102 nm).

The sintering of PS powders with higher Gd_2O_3 concentration (8, 12, and 20 mol%) was not studied for two reasons. First, based on the sintering data for PS and conventional powders (4 mol% Gd_2O_3 or Y_2O_3), it is expected that the influence of higher Gd_2O_3 concentration will show trends similar to those observed earlier [17,20] for conventional powders. Second, as described later, only the PS powder compositions described in Fig. 1 (i.e., ZrO_2-4 mol% Gd_2O_3 and YSZ) contained the metastable t′ phase, which is the phase of primary interest in the present work.

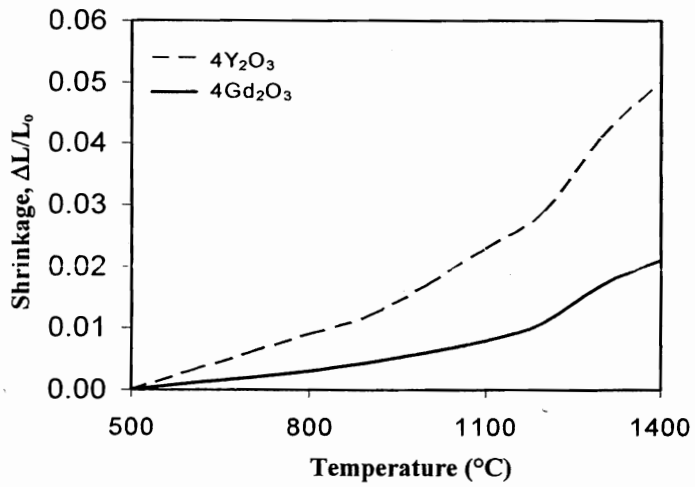

Figure 1. Shrinkage versus sintering temperature for compacts of plasma-sprayed ZrO_2-4 mol% Gd_2O_3 powder and the baseline plasma-sprayed ZrO_2–4 mol% Y_2O_3 (YSZ) powder.

Scanning electron micrographs of the fractured surfaces of compacts sintered for 0, 20, and 40 h at 1400 °C are shown in **Figure 2.** The micrographs show general indications of sintering but quantitative changes cannot be determined from the fractured surfaces. A more detailed examination with polished and thermally etched surfaces is required to evaluate microstructural changes.

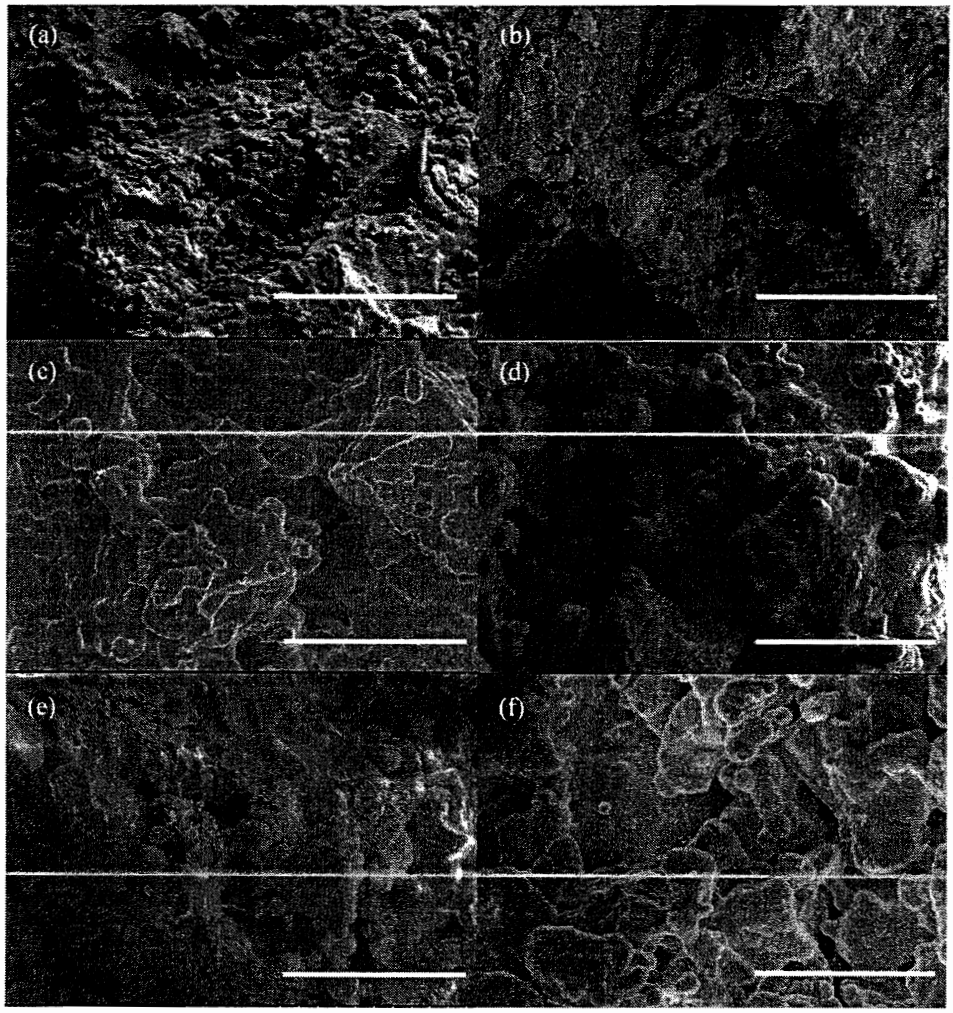

Figure 2. SEM micrographs of the fractured surfaces of plasma-sprayed powder compacts sintered at 1400 °C for various times: (a) YSZ; 0 h; (b) ZrO_2–4 mol% Gd_2O_3; 0 h; (c) YSZ; 20 h; (d) ZrO_2– 4 mol% Gd_2O_3; 20 h; (e) YSZ; 40 h; (f) ZrO_2– 4 mol% Gd_2O_3; 40 h. (Bar = 10 μm)

3.2 Phase Composition of As-Prepared Plasma-Sprayed Powders

Figure 3 shows XRD patterns of the as-prepared PS powders of Gd_2O_3-stabilized ZrO_2 (4, 8, 12, and 20 mol% Gd_2O_3) and YSZ. In the {111} region (27-33° 2θ), there is no clear evidence for the presence of monoclinic peaks in any of the patterns. In the {400} region, (70-76° 2θ), only the ZrO_2-4 mol% Gd_2O_3 and YSZ (ZrO_2-4 mol% Y_2O_3) display the t'(004) and t'(400) peaks characteristic of the t' phase. Compositions with higher Gd_2O_3 concentrations (8, 12, and 20 mol%) show a single peak characteristic of the cubic (c) phase. The data indicate that the upper boundary of the t' phase region in ZrO_2-Gd_2O_3 is somewhat below 8 mol% Gd_2O_3. **Table 1** provides a summary of the phase composition of the as-prepared PS powders.

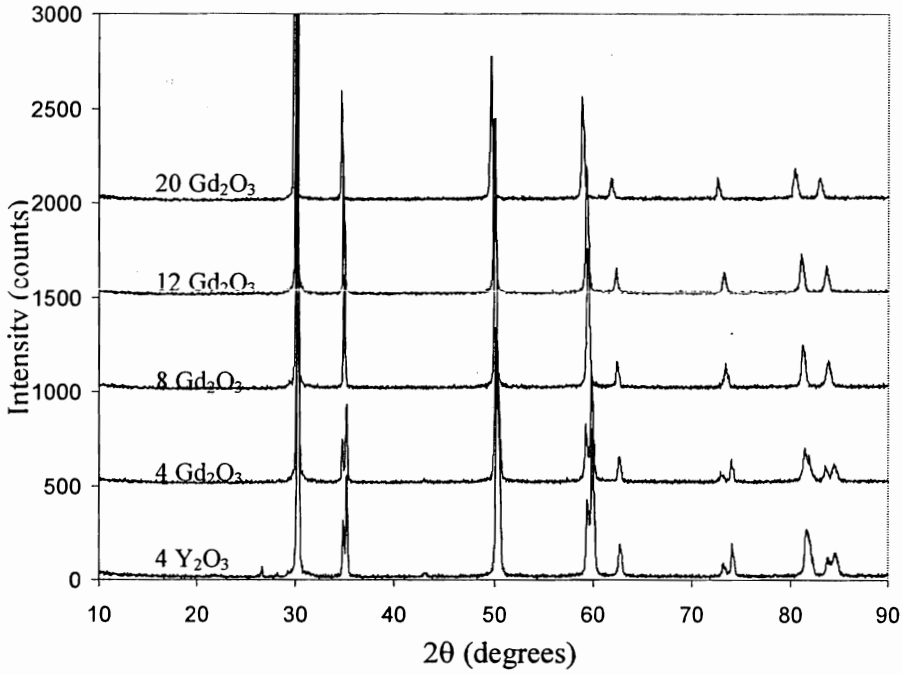

Figure 3. X-ray diffraction patterns of the as-prepared plasma-sprayed powders of Gd_2O_3-stabilized ZrO_2 powders and the baseline ZrO_2-4 mol% Y_2O_3 (YSZ) powder.

3.3 Phase Stability of Plasma-Sprayed Powders

Figure 4 shows the {111} region of plasma-sprayed ZrO_2-4 mol% Y_2O_3 (YSZ) after varying lengths of time at 1400°C and **Figure 5** shows corresponding data for ZrO_2-4 mol% Gd_2O_3. The peaks associated with the monoclinic phase in the ZrO_2-4 mol% Gd_2O_3 composition are evident after only 5 hours whereas no peaks are observed for YSZ for the same annealing time. Furthermore, for a given annealing time (40 or 80 hours) the monoclinic peaks in ZrO_2-4 mol% Gd_2O_3, relative to the t',c{111} peak, are much larger than those for YSZ. The {400} region of plasma-

Table 1. Phase composition of the as-prepared plasma-sprayed powders.

Composition	Phase	%
ZrO_2-4 mol% Y_2O_3	t'	100
ZrO_2-4 mol% Gd_2O_3	t'	100
ZrO_2-8 mol% Gd_2O_3	cubic	100
ZrO_2-12 mol% Gd_2O_3	cubic	100
ZrO_2-20 mol% Gd_2O_3	cubic	100

sprayed ZrO_2-4 mol% Y_2O_3 and for YSZ after varying annealing times at 1400°C are shown in **Figures 6 and 7**. The *t'*(004) and t'(400) peaks in ZrO_2-4 mol% Gd_2O_3 have almost disappeared for annealing times of 40 h and 80 h, whereas peaks are still noticeable for YSZ after 40 h. These data, coupled with the data in Figures 4 and 5, indicate a faster transformation (or reduced stability of the *t'* phase in ZrO_2-4 mol% Gd_2O_3, when compared to YSZ.

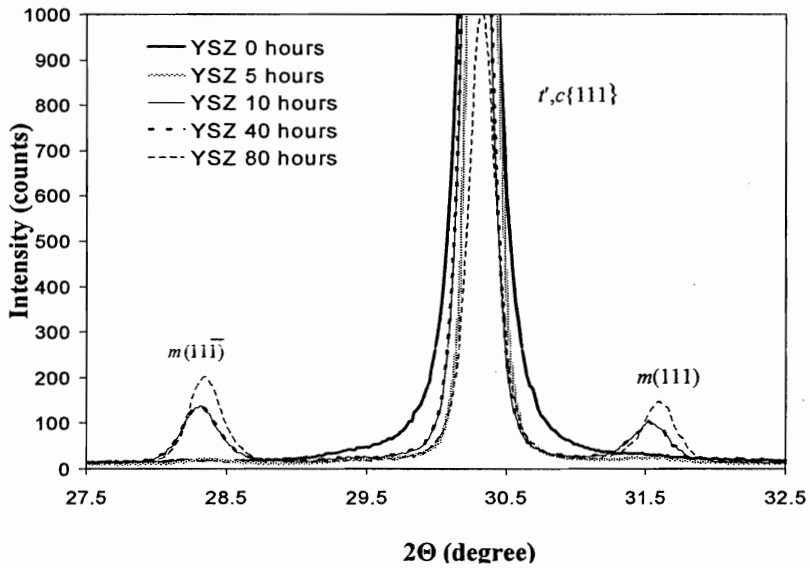

Figure 4. X-ray diffraction pattern of the {111} region of plasma-sprayed ZrO_2-4 mol% Y_2O_3 (YSZ) powder after heat treatment for 0, 5, 10, 40, and 80 hours at 1400 °C.

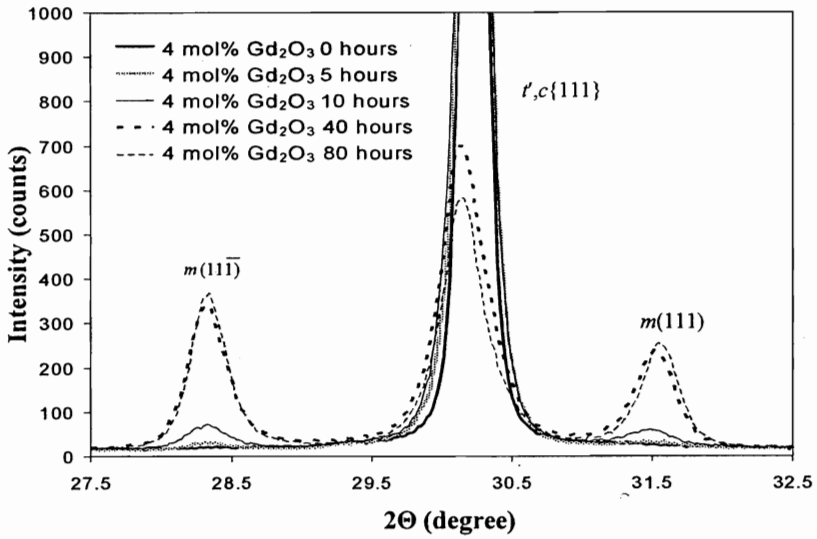

Figure 5. X-ray diffraction pattern of the {111} region of plasma-sprayed ZrO_2-4 mol% Gd_2O_3 powder after heat treatment for 0, 5, 10, 40, and 80 hours at 1400 °C.

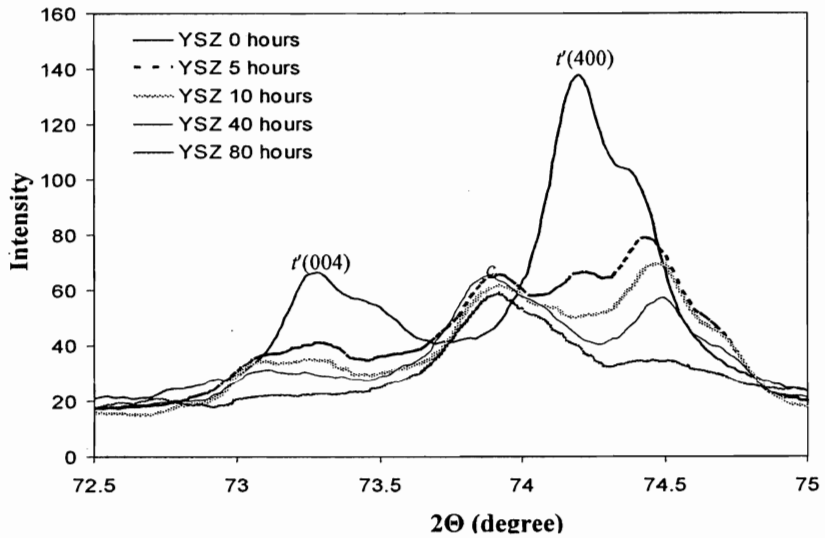

Figure 6. X-ray diffraction pattern of the {400} region of plasma-sprayed ZrO_2-4 mol% Y_2O_3 (YSZ) powder after heat treatment for 0, 5, 10, 40, and 80 hours at 1400 °C.

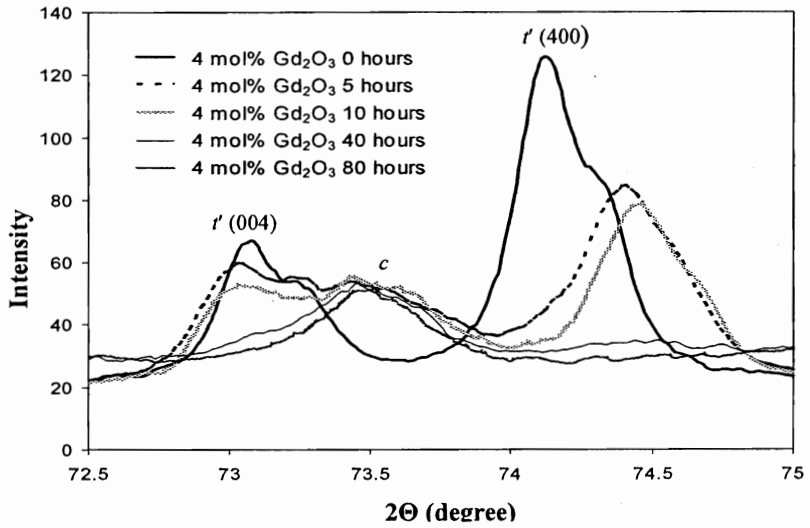

Figure 7. X-ray diffraction pattern of the {400} region of plasma-sprayed ZrO_2-4 mol% Gd_2O_3 powder after heat treatment for 0, 5, 10, 40, and 80 hours at 1400 °C.

The XRD patterns of the {111} and {400} regions (Figure 4–7) and Eq. (1) were used to determine the concentration of *m*, *c*, and *t'* phases as a function of annealing time at 1400 °C for PS powders of ZrO_2-4mol% Gd_2O_3 and YSZ. The calculated concentrations are shown in **Figures 8–10**. Each data point is the average of two samples subjected to the same annealing conditions and X-ray analysis. In the {111} region, the data for the concentration (in mol%) of *m* phase is reproducible to ±2 mol%, whereas for the {400} region, due to the overlap of the *t'* and *c* peaks, the data are reproducible to ±5 mol%. The data show that ZrO_2-4 mol% Gd_2O_3 has a lower resistance to stability of the *t'* phase when compared to YSZ. For example, after 40 h, there is no evidence for the *t'* phase in the Gd_2O_3-stabilized ZrO_2, whereas there is still ~50 mol% remaining in YSZ.

The observed decrease in the *t'* phase stability for Gd_2O_3-stabilized ZrO_2, when compared to YSZ, is consistent with the results of Rebollo *et al.* [24,25], who examined the effects of different rare-earth stabilizers on the phase stability of single-phase ZrO_2 supersaturated solid solution powders containing the t' (or c') phases. However, this is not what would be expected on the basis of kinetic considerations. The partitioning of the *t'* phase to the equilibrium *t* and *c* phases during high temperature annealing is diffusion-controlled, requiring long-range cation diffusion. The *t'* phase stability should therefore be expected to increase for Gd_2O_3-stabilized ZrO_2 compared to YSZ, because Gd^{3+} has a larger ionic radius than Y^{3+}. Rebollo *et al.* [24,25] suggested that the *t'* phase stability depends not only on the diffusion kinetics but also on the driving force for partitioning of the *t'* phase which scales as the width of the *t* + *c* phase field. Thermodynamic calculations indicate that the width of the *t* + *c* phase field scales as the radius of the rare-earth cation [26], so larger cations provide a greater driving force for partitioning. The suggestion put

forward by Rebollo *et al.* [24,25] has considerable merit but it must be remembered that phase diagrams inherently suffer from uncertainties in the phase boundaries, even for the most widely studied systems such as ZrO_2-Y_2O_3.

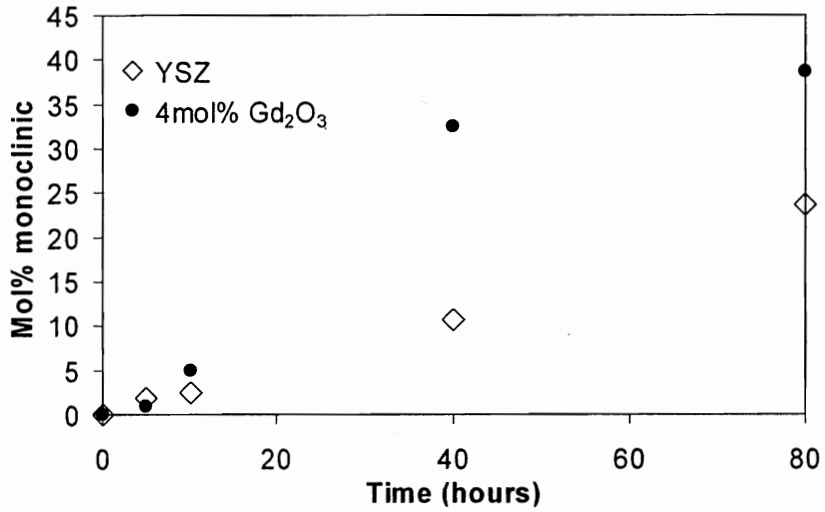

Figure 8. Concentration (mol%) monoclinic (*m*) phase versus annealing time at 1400 °C for plasma-sprayed ZrO_2-4 mol% Gd_2O_3 powder and the baseline plasma-sprayed ZrO_2-4 mol% Y_2O_3 (YSZ) powder.

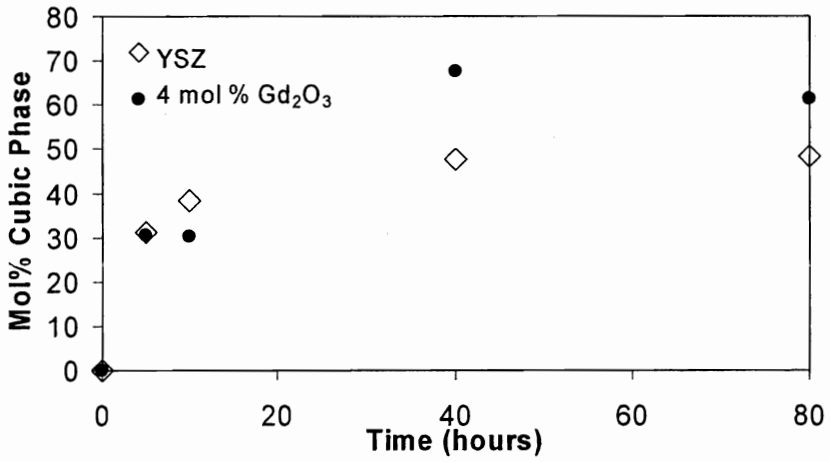

Figure 9. Concentration (mol%) cubic (*c*) phase versus annealing time at 1400 °C for plasma-sprayed ZrO_2-4 mol% Gd_2O_3 powder and the baseline plasma-sprayed ZrO_2-4 mol% Y_2O_3 (YSZ) powder.

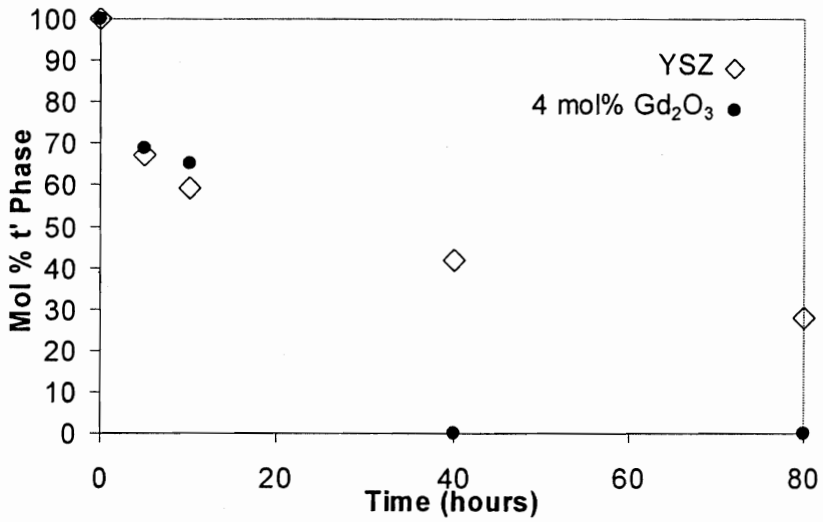

Figure 10. Concentration (mol%) *t'* phase versus annealing time at 1400 °C for plasma-sprayed ZrO_2-4 mol% Gd_2O_3 powder and the baseline plasma-sprayed ZrO_2-4 mol% Y_2O_3 (YSZ) powder.

Partitioning of the *t'* phase is complicated by several decomposition paths that are temperature dependent. It has been suggested that the formation of a Y_2O_3-rich phase, designated *t''*, occurs prior to the equilibrium *t* phase [27]. The plasma-sprayed microstructure is first replaced by a fine "tweed" microstructure resulting from a dispersion of *t''* that are spatially arranged to minimize the strain energy, followed by a classical strain-induced growth [28] of the precipitates to form a "herring bone" tiling of the tetragonal phases. The use of a large misfitting cation, such as Gd^{3+}, can provide a greater driving force for the formation of the *t''* phase, with subsequent decomposition to the *t* phase controlled by diffusional growth.

3.4 Thermal Conductivity

Figure 11 shows data for the thermal conductivity versus temperature for ZrO_2-4 mol% Y_2O_3 and YSZ fabricated from plasma-sprayed (PS) powders. The data for YSZ fabricated from conventionally-processed powders, included for comparison, are comparable to published data for conventionally-processed, hot-pressed YSZ. The lack of any significant difference between the data for PS and conventionally processed YSZ indicates that the conventionally processed materials are adequate for examining stabilizer effects on thermal conductivity. For the PS materials, ZrO_2-4 mol% Gd_2O_3 has a lower thermal conductivity than YSZ, which is consistent with published data [18].

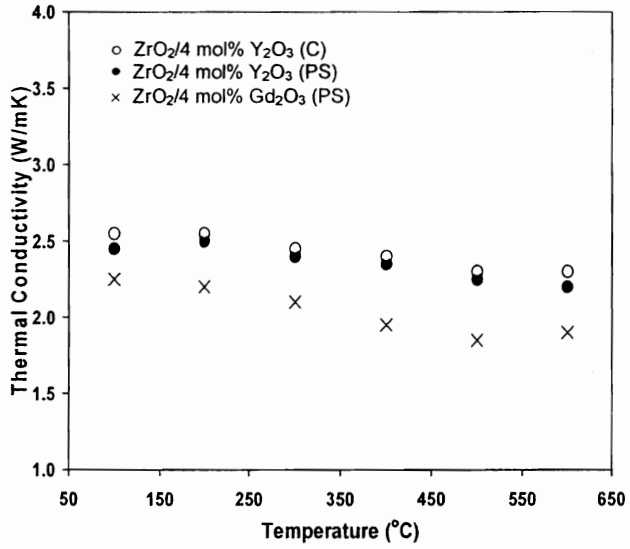

Figure 11. Thermal conductivity versus temperature for hot-pressed discs prepared from plasma-sprayed (PS) powders of ZrO_2-4 mol% Gd_2O_3 and ZrO_2-4 mol% Y_2O_3 (YSZ). For comparison, the data for YSZ prepared from conventional powder (C) is also shown.

4. SUGGESTIONS FOR FUTURE WORK

The use of Gd_2O_3 as a stabilizer for ZrO_2 is seen to provide benefits for TBC applications in the form of reduced sintering and a lowering of the thermal conductivity when compared to YSZ. An undesirable effect, however, is the reduction in the t' phase stability. Further work should examine the influence of other rare-earth stabilizers, single stabilizers as well as double dopants, on the sintering, phase stability, and thermal conductivity of plasma-sprayed ZrO_2-based materials. Ytterbium oxide, Yb_2O_3, in which the Yb^{3+} cation radius is smaller than the cation radius of Y^{3+}, is an alternative stabilizer that should be investigated. Co-doped ZrO_2 compositions, simultaneously stabilized with Y_2O_3 and another rare-earth oxide (such as Gd_2O_3 or Yb_2O_3), are worth investigating. In this way, it may be possible to combine the desirable sintering and thermal conductivity effects produced by Gd_2O_3 with the desirable t' phase stability resulting from the use of Y_2O_3. Some co-doped ZrO_2 materials have been shown to have significantly lower thermal conductivity than YSZ and a few have been found to have thermal cycle lifetimes that are comparable or superior to YSZ [9]. However, a detailed investigation of their sintering behavior, phase composition, and stability of the t' phase (if present) has not been performed.

5. CONCLUSIONS

Plasma-sprayed (PS) powders of Gd_2O_3-stabilized ZrO_2 (4 mol% Gd_2O_3) sintered more slowly and had a lower resistance to destabilization of the metastable tetragonal (t') phase than

Y_2O_3-stabilized ZrO_2 (YSZ). Gadolina-stabilized ZrO_2 (4 mol% Gd_2O_3) also had a lower thermal conductivity than YSZ. Since sintering and the partitioning of the t' phase to the equilibrium tetragonal (t) and cubic (c) phases are diffusion-controlled, the role of the larger Gd^{3+} ion in lowering both the sintering and t' phase stability cannot be explained in terms of kinetics only. The driving force for the partitioning of the t' phase must also be considered. The factors influencing the driving force are currently not clear because the decomposition of the t' phase is complicated by several temperature-dependent decomposition paths. Practically, Gd_2O_3 by itself may not be an effective stabilizer for ZrO_2-based TBCs intended for high temperature use. Future work should investigate the sintering, phase stability, and thermal conductivity of co-doped ZrO_2 compositions simultaneously stabilized with Y_2O_3 and another rare-earth oxide such as Gd_2O_3.

REFERENCES

[1]T. E. Strangman, "Thermal Barrier Coatings for Airfoils," Thin Solid Films, 127, 93-105 (1985).

[2]R. A. Miller, "Ceramic Thermal Barrier Coatings," Surf. Coat. Technol., 30, 1-11 (1987).

[3]J. T. DeMasi-Marcin and D. K. Gupta, "Protective Coatings in the Gas Turbine Engine," Surface Coat. Technol., 168-169, 1-9 (1994).

[4]R. A. Miller, "Thermal Barrier Coatings for Aircraft Engines – History and Directions." In: Thermal Barrier Coating Workshop, NASA Conference Publication 3312 (1995), pp. 17-34.

[5]R. V. Hillery, "Coatings for High Temperature Structural Materials: Trends and Opportunities." National Materials Advisory Board Report, National Academy Press, Washington, DC (1996).

[6]M. J. Stiger, N. M. Yanar, M. G. Topping, F. S. Pettit, and G. H. Meier, "Thermal Barrier Coatings for the 21st Century," Z. Metallkd., 90[12], 1069-1068 (1999).

[7]D. Zhu and R. A. Miller, "Thermal Barrier Coatings for Advanced Gas Turbine Engines," MRS Bulletin, 27[7], 43-47 (2000).

[8]D. R. Clarke and C. G. Levi, "Materials Design for the Next Generation Thermal Barrier Coatings," Annu. Rev. Mater. Res., 33, 383-417 (2003).

[9]D. Zhu, and R. A. Miller, "Thermal Conductivity and Sintering Behavior of Advanced Thermal Barrier Coatings," Ceram. Eng. Sci. Proc., 23[4], 457-468 (2002).

[10]D. Zhu, and R. A. Miller, "Sintering and Creep Behavior of Plasma-Sprayed Zirconia- and Hafnia-Based Thermal Barrier Coatings," Surf. Coat. Technol., 108-109, 114-120 (1998).

[11]P. A. Langjahr, R. Oberacker, and M. J. Hoffmann, "Long-term Behavior and Application Limits of Plasma-Sprayed Zirconia Thermal Barrier Coatings," J. Am. Ceram. Soc., 84[6], 1301-1308 (2001).

[12]V. Lughi, V. K. Tolpygo, and D. R. Clarke, "Microstructural Aspects of the Sintering of Thermal Barrier Coatings," Mater. Sci. Eng., A368, 212-221 (2004).

[13]R. A. Miller, J. L. Smialek, and R. G. Garlick, "Phase Stability in Plasma-Sprayed Partially Stabilized Zirconia-Yttria." In: Advances in Ceramics, Vol. 3, Science and Technology of Zirconia. Edited by A. H. Heuer and L. W. Hobbs. The American Ceramic Society, Columbus, OH (1981), pp. 241-253.

[14]R. A. Miller, R. G. Garlick, and J. L. Smialek, "Phase Distributions in Plasma-Sprayed Zirconia-Yttria," Am. Ceram. Soc. Bull., 62[12], 1355-1358 (1983).

[15]R. Chaim, D. G. Brandon, and A. H. Heuer, "A Diffusional Phase Transformation in ZrO_2–4 wt% Y_2O_3 Induced by Surface Segregation," Acta Metall., 34[10], 1933-1939 (1986).

[16]U. Schulz, "Phase Transformation in EB-PVD Yttria Partially Stabilized Zirconia Thermal Barrier Coatings," J. Am. Ceram. Soc., 83[4], 904-910 (2000).

[17]M. N. Rahaman and J. R. Gross, "Thermal Barrier Coatings," TOPS DO 0007 Report, September, 2003.

[18]J. R. Nicholls, K. J. Lawson, A. Johnstone, and D. S. Rickerby, "Low Thermal Conductivity EB-PVD Coatings," Mater. Sci. Forum, 369-372, 595-606 (2001).

[19]R. D. Shannon and C. T. Prewitt, "Effective Ionic radii in oxides and Fluorides," Acta Cryst., B25, 925-946 (1969).

[20]J. R. Gross, M. N. Rahaman, and R. E. Dutton, "Sintering, Grain Growth, and Phase Composition of Gd_2O_3-Stabilized ZrO_2," Ceram. Trans., 154, 311-320 (2003).

[21]J. Wu, X. Wei, N. P. Padture, P. G. Clemens, M. Gell, E. Garcia, P. Mirano, M. I. Osendi, "Low Thermal Conductivity Rare-Earth Zirconates for Potential Thermal-Barrier-Coating Applications," J. Am. Ceram. Soc., 85[12], 3031-3035 (2002).

[22]L. M. Clark and R. E. Taylor, "Radiation Loss in the Flash Method for Thermal Diffusivity," J. Appl. Phys., 46, 714-719 (1975).

[23]R. E. Taylor, "Thermal Conductivity Determinations of Thermal Barrier Coatings," Mater. Sci. Eng., A245, 160-167 (1998).

[24]N. R. Rebollo, O. Fabrichnaya, and C. G. Levi, "Phase Stability of Y + Gd Co-Doped Zirconia," Z. Metallkd., 94[3], 163-170 (2003).

[25]N. R. Rebollo, A. S. Gandhi, and C. G. Levi, "Phase stability issues in emerging TBC systems," In: Proceedings of the Electrochemcial Society: High Temperature Corrosion and Materials Chemistry IV. Edited by E. Opila, P. Hou, T. Maruyama, B. Pieraggi, M. McNallan, D. Shifler, and E. Wuchina, (2003), pp. 431-442.

[26]H. Yokokawa, N. Sakai, T. Kawada, and M. Dokiya, "Phase Diagram Calculations for ZrO_2 Based Ceramics: Thermodynamic Regularities in Zirconate Formation and Solubilities of Transition Metal Oxides," In: Science and Technology of Zirconia V. Edited by S. P. S. Badwal, M. J. Bannister, and R. H. J. Hannink. Technomic Publising, Lancaster, Australia, (1993), pp. 59-68.

[27]L. Lelait, S. Alpérine, C. Diot, and M. Mévrel, "Thermal Barrier Coatings: Microstructural Investigation after Annealing" Mater. Sci. Eng., A121, 475-482 (1989).

[28]A. G. Katchaturyan, Theory of Structural Transformations in Solids. Wiley, New York (1983).